Compositional variation of pyroxene and mica from the Little Murun ultrapotassic complex, Aldan Shield, Russia

ROGER H. MITCHELL

Department of Geology, Lakehead University, Thunder Bay, Ontario, Canada P7B 5E1

AND

NIKOLAI V. VLADYKIN

Vinogradov Institute of Geochemistry, Russian Academy of Science, P.O. Box 4019, Irkutsk-33, Russia 664033

Abstract

Pyroxene and mica found in plutonic rocks of the Little Murun ultrapotassic pluton exhibit trends of compositional evolution that permit evaluation of the differentiation sequence of the complex. Pyroxene evolves from diopside in kalsilite and phlogopite pyroxenites through aegirine-diopside in shonkinite to aegirine in late stage charoitite and evolved hypabyssal rocks. The compositional trend is unusual in that the hedenbergite content of the pyroxenes never exceeds 15 mol.% and is thus unlike pyroxene compositional trends found in sodic alkaline complexes. Mica is Al- and Ti-poor and ranges in composition from Fe-rich phlogopite through biotite towards tetraferriannite. Compositional trends of mica found in 'lamproite-like' hypabyssal rocks are identical to those observed in the micaceous plutonic rocks; hence the former are considered to be representatives of the lamprophyric facies of the magmas which formed the plutonic series.

KEYWORDS: diopside, phlogopite, kalsilite, ultrapotassic, alkaline complex, Yakutia, Russia.

Introduction

THE Little Murun ultrapotassic complex is one of several large Mesozoic potassic alkaline complexes emplaced in the Aldan shield of eastern Siberia (Bilibina *et al.*, 1967; Kostyuk *et al.*, 1990; Kogarko *et al.*, 1995). Little Murun is the largest of a group of three alkaline complexes located to the south of the town of Olekminsk (Fig. 1). The complex is of mineralogical and petrological importance as it contains rocks of very unusual mineralogy and composition, e.g. charoitites, pyroxene-kalsilitolites (yakutites) etc., and because some Russian scientists consider that it contains both plutonic and effusive lamproites (Vladykin, 1985; Shadenkov *et al.*, 1990).

Most previous mineralogical studies of the complex have concentrated upon the exotic mineralogy of the rocks and few data are available concerning the compositions of the common rock forming silicates. Accordingly we have undertaken a systematic study of the compositional variation of clinopyroxene and mica from the Little Murun intrusion with the principal object of assessing the relationships between the major rock types which have been proposed on the basis of field relationships. This approach is necessary as the complex, in common with many other alkaline complexes, is extremely heterogeneous (on the scale of decametres) and very poorly-exposed. Hence, is not possible to determine from simple field mapping the actual structure of the complex or the delineate the intrusive relationships between the diverse syenites present. Material obtained from shallow drill holes cannot be correlated because of these gross lithological variations. Consequently, we regard the hypothesis of Orlova (1988), that the structure of the complex is lopolithic, as highly improbable. A second objective of the study is to provide comparative data for the compositional evolution of pyroxene in ultrapotassic plutonic rocks relative to those found in sodic alkaline complexes.
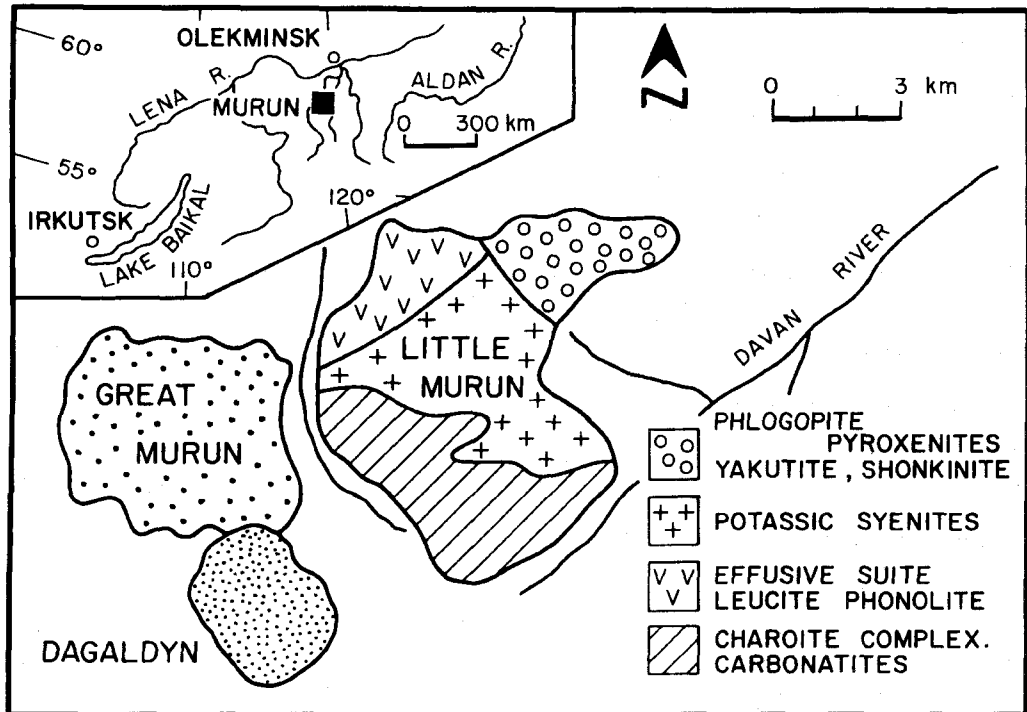
FIG. 1. Location and geological sketch map of the Little Murun alkaline complex, after Orlova *et al.* (1992) and
Konyev *et al.* (1993).

Four distinct series, or centres, of alkaline rocks
occur in the complex (Fig.1; Orlova, 1988; Vladykin,
1990; Orlova *et al.*, 1992): (I) an ultrabasic suite
consisting of phlogopite pyroxenite, kalsilite syenite
and kalsilite pyroxenite (yakutite and synnyrite;
Zhidkov and Smyslov, 1985; Smyslov, 1986) and
shonkinite; (II) diverse potassium feldspar-bearing
syenites including pseudoleucite syenite, shonkinite
and fergusonite; (III) a volcanic series consisting of
leucite tinguaite, phonolite, solvsbergite and trachyte;
(IV) a charoitite-carbonatite complex. Each centre
exhibits extraordinary complexity and the sequence
of intrusion with each centre is difficult to determine.
However, on the basis of field relationships the
evolutionary sequence for the complex as a whole is
considered to be in the order given above.

The volcanic rocks represent a high level carapace
that has been down-faulted into the plutonic series.
Unfortunately, the majority of these are highly-
altered and unsuitable for geochemical and/or
mineralogical studies which might aid in the
identification of parental magmas. The lavas and
centre I plutonic rocks have been intruded by dykes
and sills of complex mineralogy. These include: (1)
phlogopite-rich 'lamproite-like' rocks which contain
potassium batisite, potassium richterite and wadeite;
(2) agpaitic dykes with kalsilite, potassium feldspar,
barytolamprophyllite and eudialyte; (3) tausonite-,
wadeite- and barytolamprophyllite-bearing dykes.

The carbonatite complex is unlike plutonic calcite/
dolomite carbonatites associated with sodic alkaline
complexes and contains rocks composed of Sr-Ca-Ba
carbonate (barytocalcite, benstonite, strontianite,
burbankite) and aegirine, quartz-carbonate rocks,
tinaksite-microcline rocks, together with modally
diverse assemblages of charoite, tinaksite, canasite,
carbonates, aegirine and potassium feldspar
(Vladykin, 1990). Depending upon the mode these
rocks are known locally as murunite, ditmarite,
torgoite and charoitite (Alekseyev, 1983; Prokofiev
and Vorobyev, 1992). Many members of the
charoitite-carbonatite complex are considered to be
'fenites' or rocks formed by metasomatic processes
(Orlova, 1988; Ivanyuk and Evdokimov, 1991;
Biryukov and Berdnikov, 1993).

Analytical techniques

Mineral compositions were determined at Purdue
University using an automated Cameca SX-50

TABLE 1. Representative compositions of pyroxene from kalsilite pyroxenite

wt.%	1	2	3	4	5	6	7	8	9
SiO_2	54.13	54.15	53.46	53.54	52.06	52.31	54.11	54.57	54.06
TiO_2	0.14	0.29	0.19	0.08	0.30	0.19	0.19	0.12	0.16
Al_2O_3	0.27	0.22	0.27	0.68	2.26	0.93	0.31	0.11	0.09
Cr_2O_3	0.14	0.03	0.15	0.03	0.02	n.d.	0.17	0.19	0.06
FeO_T	3.74	4.72	6.04	5.52	5.87	6.95	3.35	5.59	7.93
MnO	0.12	0.08	0.14	0.07	0.17	0.18	0.07	0.13	0.25
MgO	16.27	15.84	15.26	15.04	14.56	14.21	16.78	14.94	13.59
CaO	23.96	23.69	23.44	23.94	24.89	24.59	24.63	23.69	22.01
Na_2O	0.66	0.88	1.14	0.34	0.41	0.37	0.17	0.78	1.81
Total	99.54	99.90	100.06	100.26	100.57	99.75	99.79	100.14	99.97

Recalculated compositions on the basis of stoichiometry

Fe_2O_3	1.96	2.73	5.11	2.04	3.62	3.29	0.89	1.06	4.68
FeO	1.98	2.27	1.44	3.69	2.61	3.99	2.55	4.63	3.72
Total	99.60	100.17	100.60	100.44	100.90	100.06	99.87	100.23	100.43

Structural formulae calculated on the basis of 4 cations and 6 oxygen

Si	1.985	1.981	1.957	1.967	1.907	1.942	1.979	2.005	1.993
Al	0.012	0.009	0.012	0.029	0.098	0.041	0.013	0.005	0.004
Ti	0.004	0.008	0.005	0.002	0.008	0.005	0.005	0.003	0.004
Cr	0.004	0.001	0.004	0.001	0.001	–	0.005	0.006	0.002
Fe^{3+}	0.054	0.075	0.141	0.056	0.100	0.092	0.024	0.029	0.130
Fe^{2+}	0.061	0.069	0.044	0.113	0.080	0.124	0.078	0.142	0.115
Mn	0.004	0.002	0.004	0.002	0.005	0.006	0.002	0.004	0.008
Mg	0.889	0.864	0.833	0.823	0.795	0.786	0.917	0.818	0.747
Ca	0.947	0.928	0.919	0.982	0.977	0.978	0.965	0.932	0.869
Na	0.047	0.062	0.081	0.024	0.029	0.027	0.012	0.056	0.129

Mol.% end-members

TiPx	0.39	0.47	0.52	0.22	0.82	0.53	0.52	0.01	0.20
CATS	–	–	–	0.14	1.66	–	–	–	–
Ae	4.70	6.23	8.00	2.42	2.90	2.65	1.21	5.62	12.99
Wo	46.96	46.10	45.18	48.33	47.46	48.34	48.00	47.15	43.54
Fs	3.39	4.09	5.14	7.26	7.51	9.40	4.52	5.87	5.78
En	44.56	43.11	41.16	41.63	39.64	39.09	45.75	41.37	37.50

Projection from Wo into Ae-Hd-Di

Ae	4.48	5.94	7.64	2.34	3.86	2.55	1.13	5.39	12.56
Hd	6.76	8.15	10.25	14.65	15.48	18.89	8.89	11.76	11.68
Di	88.76	85.91	82.11	83.01	81.66	78.56	89.97	82.85	75.76

FeO_T = total Fe calculated as FeO; n.d. = not detected.
TiPx = $CaTiAl_2O_6$; CATS = $CaAl(Si,Al)O_6$; Ae = aegirine; Wo = wollastonite;
Fs = ferrosilite; En = enstatite; Hd = hedenbergite; Di = diopside.
Compositions; 1–3, sample 172; 4–6, sample 229; 7–9, sample 187/2.

wavelength dispersive microprobe. Standards employed were natural minerals or synthetic compounds and glasses. Standard operating conditions were 15 kV and 20 nA. Major elements are correct to with $\pm 2\%$ of the element weight present. Minor elements are less accurately determined but are reproducible to within 0.05 wt.%. Representative compositions of pyroxene and mica are given in Tables 1–4 and 5–8, respectively.

Representative compositions of pyroxene are given in Tables 1–4. Structural formulae, ferric and ferrous iron contents were calculated on the basis of

TABLE 2. Representative compositions of pyroxene from phlogopite pyroxenites and centre-I shonkinites

wt.%	1	2	3	4	5	6	7	8	9
SiO_2	54.95	54.41	54.38	53.47	53.47	53.24	53.89	53.54	54.21
TiO_2	0.18	0.17	0.18	0.08	0.28	0.31	0.29	0.15	0.33
Al_2O_3	0.37	0.11	0.09	0.07	0.37	0.12	0.16	0.18	0.14
Cr_2O_3	n.d.	0.15	0.05	0.13	n.d.	0.19	0.04	0.04	0.04
FeO_T	3.45	5.44	7.28	9.65	12.41	13.77	15.28	6.58	14.78
MnO	0.12	0.21	0.22	0.21	0.31	0.30	0.41	0.31	0.22
MgO	16.88	14.92	13.78	13.13	10.67	9.56	8.83	14.54	9.09
CaO	24.85	24.27	22.33	20.23	18.12	16.37	15.58	21.52	15.88
Na_2O	0.10	0.61	1.49	2.99	3.50	4.88	5.38	1.59	5.19
Total	100.89	100.47	99.87	99.96	99.43	98.91	99.88	98.45	99.89

Recalculated compositions on the basis of stoichiometry

Fe_2O_3	0.10	1.06	2.66	10.03	7.77	11.97	12.93	4.00	11.66
FeO	3.36	4.49	4.89	0.63	5.41	3.00	3.64	2.98	4.29
Total	100.91	100.40	100.07	100.95	100.11	99.94	101.16	98.85	101.05

Structural formulae calculated on the basis of 4 cations and 6 oxygens

Si	1.989	1.998	2.009	1.962	1.997	1.994	2.001	1.993	2.011
Al	0.016	0.005	0.004	0.003	0.025	0.005	0.007	0.008	0.006
Ti	0.005	0.005	0.005	0.002	0.008	0.009	0.008	0.004	0.009
Cr	–	0.004	0.001	0.004	–	0.006	0.001	0.001	0.001
Fe^{3+}	0.003	0.029	0.074	0.277	0.219	0.337	0.361	0.112	0.326
Fe^{2+}	0.102	0.138	0.151	0.019	0.169	0.094	0.113	0.093	0.133
Mn	0.004	0.007	0.007	0.007	0.010	0.010	0.013	0.010	0.007
Mg	0.991	0.817	0.759	0.718	0.594	0.534	0.489	0.807	0.503
Ca	0.964	0.955	0.884	0.795	0.725	0.657	0.620	0.858	0.631
Na	0.007	0.043	0.107	0.213	0.253	0.354	0.387	0.115	0.373

Mol.% end-members

TiPx	0.49	0.23	0.10	0.15	0.44	0.27	0.18	0.39	0.20
CATS	0.15	–	–	–	–	–	–	–	–
Ae	0.70	4.33	10.82	21.02	25.80	35.81	39.28	11.54	38.01
Wo	48.04	48.00	44.88	39.21	36.68	33.06	31.34	42.96	32.31
Fs	4.89	6.23	5.99	4.12	6.83	3.89	4.42	4.53	4.34
En	45.72	41.16	38.47	35.50	30.24	26.97	24.79	40.58	25.60

Projection from Wo into Ae-Hd-Di

Ae	0.66	4.23	10.43	20.26	24.99	35.71	39.16	10.91	37.80
Hd	9.60	12.59	12.07	8.30	10.82	8.10	9.21	8.95	9.02
Di	89.74	83.18	77.50	71.45	61.19	56.19	51.63	80.14	53.18

FeO_T = total Fe calculated as FeO; n.d. = not detected
TiPx = $CaTiAl_2O_6$; CATS = $CaAl(Si,Al)O_6$; Ae = aegirine; Wo = wollastonite; Fs = ferrosilite; En = enstatite;
Hd = hedenbergite; Di = diopside.
1–7 biotite pyroxenite; 8–9 shonkinite. 1, 187/3; 2, 187/5; 3, M1;
4, M4; 5–6, 183; 7, 120/9; 9, 144/8.

stoichiometry using the method of Droop (1987). End-member component pyroxenes listed in Tables 1–4 have been calculated by combining all the Na present with an equivalent of amount of Fe^{3+} as aegirine. This procedure has been shown to be reasonable for Ti and Al-poor pyroxenes found in alkaline rocks as wet chemical analyses have shown them to be essentially members of the aegirine–hedenbergite–diopside solid solution series (Mitchell and Platt, 1982; Mitchell, 1980; Tyler and King, 1967).

Representative compositions of mica and amphibole are given in Tables 5—9. Structural formulae, ferric and ferrous iron contents have been calculated on the basis of stoichiometry using the method of Droop (1987). It should be realized that for mica only minimum estimates of Fe^{3+} contents may be obtained by this procedure. Mica compositions in many instances do not, on the basis of the recalculation scheme used, contain any Fe_2O_3 as a consequence of containing fewer than 16 cations/formula unit. These low totals, and hence the apparent absence of Fe_2O_3 may result from A-site cation deficiencies related to either incipient alteration or the presence of light elements, e.g. lithium, which cannot be determined by electron microprobe techniques. The slightly low alkali contents relative to the ideal amounts in mica do not result from volatilization of potassium during analysis under the analytical conditions employed. Fortunately, exact determination of Fe^{3+} content is not critical for the purposes of this paper as comparisons are made primarily on the basis of oxide contents versus total Fe expressed as FeO.

Pyroxene compositional variation

Centre-I. Pyroxene in phlogopite kalsilite pyroxenite (yakutite) is anhedral brown to greenish diopside which exhibits very limited compositional variation (Table 1; Fig 2). Oscillatory or sector zoning is absent and minor Fe-enrichment is confined to irregular zones at the margins of the crystals. Optically, this is manifested by increasing green pleochroism. These pyroxenes are the least evolved in the complex, with respect to their Na, Fe^{2+} and Fe^{3+} contents. Individual samples are characterized by pyroxene of a particular restricted compositional range (Fig. 2). The overall trend is limited to about 15 mol.% diopside and compositions lie close to the diopside-hedenbergite (Di-Hd) join. The weak zonation to aegirine-bearing margins shown by pyroxene in phlogopite potassium feldspar kalsilite pyroxenite (synnyrite; sample 187/2), may reflect subsolidus reequilibration with deuteric fluids. TiO_2 (0.1—0.6 wt.%) and Al_2O_3(0.1—2.3 wt.%) are low, consequently $CaTiAl_2O_6$ and $CaAl(SiAl)O_6$ contents are less than 1 and 2 mol.%, respectively (Table 1). Cr contents are negligible.

Clinopyroxene in phlogopite pyroxenite occurs as anhedral brownish-green to green pleochroic crystals. Increasing intensity of pleochroism is correlated with increasing Fe^{3+} content. Representative compositions are given in Table 2, which indicates that the pyroxenes are poor in TiO_2 (0.02—0.4 wt.%) and Al_2O_3 (0.1—0.7 wt.%) and are hedenbergite-poor (<15 mol.%) members of the diopside–aegirine solid solution series. Individual samples exhibit distinct ranges of composition, although the overall evolutionary trend is similar (Fig. 3). Diopside-rich cores are similar in composition to unevolved pyroxene in kalsilite pyroxenite.

Pyroxene in centre-I shonkinite primarily occurs as bright green weakly-zoned anhedral crystals. However, a few samples contain crystals zoned from brownish-green cores to green margins. Representative compositions are given in Table 2. The pyroxenes are poor in TiO_2 (0.1—0.5 wt.%) and Al_2O_3 (0.1—0.2 wt.%) and are aegirine–diopside solid solutions which contain <15 mol. % hedenbergite (Fig. 4).

Centre-II. Pyroxene in centre-II shonkinite and syenite occurs as bright green weakly-zoned crystals. Representative compositions (Table 3) indicate that they are TiO_2 (0.1—0 wt.%) and Al_2O_3 (0.1—0.4 wt.%)-poor intermediate members of the aegirine–diopside solid solution series. Individual samples exhibit discrete ranges in composition although their
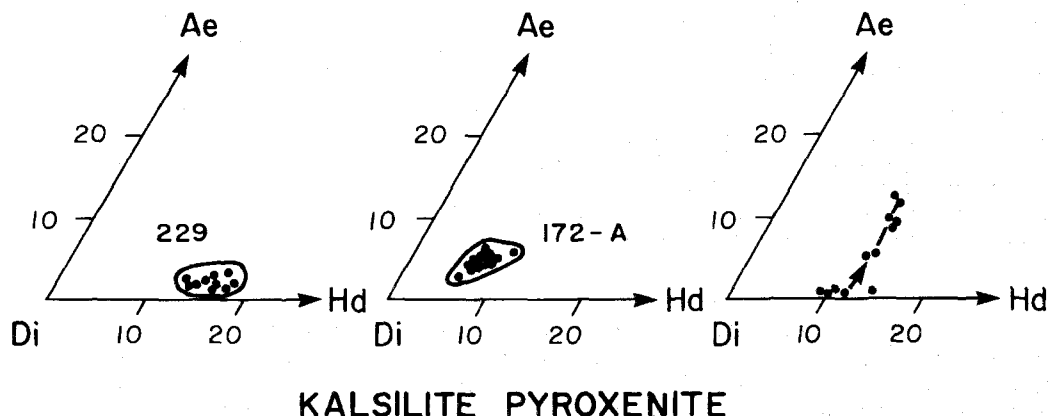

KALSILITE PYROXENITE

FIG. 2. Compositional variation of pyroxene in kalsilite pyroxenites.

TABLE 3. Representative compositions of pyroxene from centre-II shonkinites and syenites

| wt.%	1	2	3	4	5
SiO_2	52.88	53.11	52.90	52.40	52.97
TiO_2	0.12	0.13	0.45	0.18	0.18
Al_2O_3	0.29	0.09	0.24	0.19	0.10
Cr_2O_3	n.d.	0.05	n.d.	n.d.	n.d.
FeO_T	14.92	17.98	21.01	22.39	24.88
MnO	0.29	0.22	0.31	0.33	0.12
MgO	8.95	7.15	5.07	4.06	2.98
CaO	17.02	12.75	11.08	8.77	5.95
Na_2O	4.22	6.55	7.55	8.57	10.05
Total	98.92	98.18	98.70	97.01	97.28
Recalculated compositions					
Fe_2O_3	10.22	15.59	17.67	20.13	22.56
FeO	5.72	3.95	5.11	4.28	4.56
Total	99.71	99.59	100.38	98.91	99.09
Structural formulae (4 cations/6 oxygens)					
Si	1.999	2.012	2.007	2.019	2.040
Al	0.013	0.004	0.011	0.009	0.005
Ti	0.003	0.004	0.013	0.005	0.005
Cr	–	0.005	–	–	–
Fe^{3+}	0.291	0.444	0.505	0.584	0.655
Fe^{2+}	0.181	0.125	0.162	0.138	0.147
Mn	0.009	0.007	0.010	0.011	0.004
Mg	0.504	0.404	0.287	0.233	0.148
Ca	0.689	0.517	0.450	0.362	0.246
Na	0.309	0.481	0.555	0.640	0.751
Mol.% end-members					
TiPx	0.19	0.29	0.06	0.30	0.30
CATS	–	–	–	–	–
Ae	31.30	48.66	56.68	65.39	56.09
Wo	34.78	26.23	22.95	18.48	22.84
Fs	8.21	4.50	5.68	4.16	6.80
En	25.52	20.31	14.63	11.67	14.07
Projection from Wo into Ae-Hd-Di					
Ae	30.75	48.33	57.19	66.09	55.97
Hd	16.86	9.29	11.96	8.76	14.24
Di	52.39	42.38	30.85	25.15	29.79

FeO_T = total Fe calculated as FeO; n.d. = not detected; TiPx = $CaTiAl_2O_6$;
CATS = $CaAl(Si,Al)O_6$; Ae = aegirine; Wo = wollastonite; Fs = ferro-silite;
En = enstatite; Hd = hedenbergite; Di = diopside.
Compositions; 1–2, shonkinite 158; 3, biotite garnet syenite 105;
4–5, biotite pyroxene syenite 191/5.

overall trends of evolution are similar (Fig. 5). The pyroxenes are more evolved, i.e. richer in aegirine than similar pyroxene in centre-I shonkinite.

Centre-III. Tinguaite and leucitophyre considered to be representative of centre-III effusives contain strongly-zoned subhedral bright green micropheno-crystal pyroxene. These range in composition from diopsidic aegirine to aegirine (Table 4, Fig. 6).

Late-stage mineralogically complex dykes contain anhedral to subhedral weakly-zoned bright green
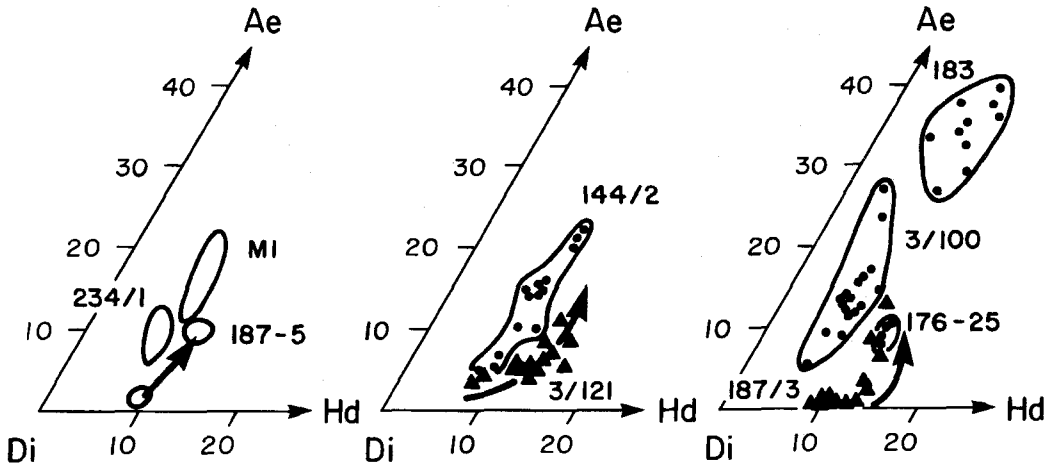
PHLOGOPITE – PYROXENITES – I

FIG. 3. Compositional variation of pyroxene in phlogopite pyroxenites.

pleochroic pyroxene. Some rocks contain spray-like aggregates of thin prismatic crystals. In the majority of samples the pyroxene is nearly-pure aegirine (Table 4, Fig. 6) which is very poor in Al_2O_3 (<0.3 wt.%). TiO_2 contents are variable within and between samples. Typically, TiO_2 ranges from 0.2–0.5 wt.%, but may reach up to 2.8 wt.% (Table 5) in rocks containing K-titanosilicates. The Ti-rich pyroxenes, with Ti>Al, undoubtedly contain significant amounts of the $Na(X_{0.5},Ti_{0.5})Si_2O_6$ (X = Mg, Mn, Fe^{2+}) pyroxene end-members in solid solution (see below). Similar aegirine-rich pyroxene is present in magnesio-arfvedsonite–biotite-bearing veins (Ch 3/100) which cut centre-I biotite pyroxenite.
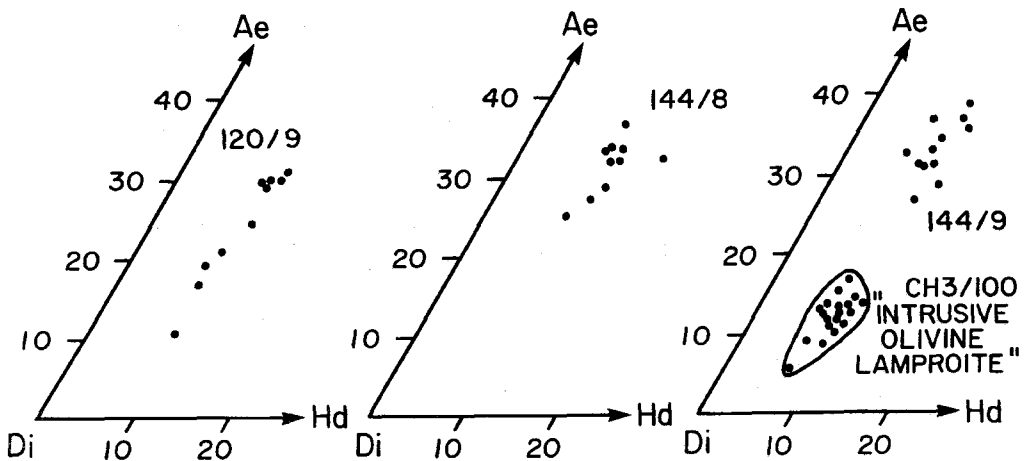
SHONKINITES – I

FIG. 4. Compositional variation of pyroxene in centre-I shonkinites and sample Ch 3/100. The latter is an olivine-bearing phlogopite pyroxenite previously described (Panina et al., 1990) as a intrusive olivine lamproite.

TABLE 4. Representative compositions of pyroxene from centre-III syenites, centre-III effusive rocks and benstonite carbonatites of the charoite complex

wt.%	1	2	3	4	5	6	7	8	9
SiO_2	51.69	52.08	52.57	53.05	53.11	52.37	51.85	53.06	51.95
TiO_2	1.39	0.29	0.24	0.12	0.24	0.07	0.81	0.29	0.38
Al_2O_3	0.18	0.15	0.22	0.39	0.23	0.21	0.40	n.d.	n.d.
Cr_2O_3	n.d.	n.d.	n.d.	n.d.	n.d.	n.d.	n.d.	n.d.	n.d.
FeO_T	23.96	25.92	27.79	29.13	25.58	27.89	31.06	22.59	25.27
MnO	0.35	0.19	0.22	0.35	0.40	0.19	n.d.	0.30	0.61
MgO	2.83	2.38	1.15	0.23	2.07	1.01	0.60	4.24	2.08
CaO	7.39	5.66	2.97	1.53	6.73	3.63	0.27	9.00	10.14
Na_2O	9.20	10.56	11.61	12.57	9.49	11.37	13.29	8.46	7.71
Total	97.06	96.78	96.71	97.13	97.92	96.93	98.47	98.02	98.30

Recalculated compositions on the basis of stoichiometry

	1	2	3	4	5	6	7	8	9
Fe_2O_3	20.48	26.71	27.36	29.56	20.65	27.30	34.24	19.34	17.64
FeO	5.53	1.89	3.17	2.53	7.00	3.32	0.25	5.19	9.40
Total	99.04	99.91	99.51	100.33	99.92	99.48	101.89	99.78	99.91

Structural formulae calculated on the basis of 4 cations and 6 oxygens

	1	2	3	4	5	6	7	8	9
Si	2.002	1.995	2.205	2.208	2.043	2.022	1.959	2.027	2.221
Al	0.004	0.007	0.010	0.018	0.010	0.010	0.018	–	–
Ti	0.008	0.008	0.007	0.003	0.007	0.002	0.025	0.008	0.011
Fe^{3+}	0.597	0.770	0.793	0.850	0.598	0.793	0.974	0.556	0.517
Fe^{2+}	0.179	0.060	0.102	0.081	0.225	0.107	0.008	0.166	0.306
Mn	0.011	0.006	0.007	0.011	0.013	0.006	–	0.006	0.020
Mg	0.163	0.136	0.066	0.013	0.119	0.058	0.034	0.241	0.121
Ca	0.307	0.232	0.123	0.063	0.277	0.150	0.011	0.368	0.423
Na	0.691	0.784	0.867	0.932	0.708	0.851	0.974	0.627	0.582

Mol. % end-members

	1	2	3	4	5	6	7	8	9
TiPx	0.42	0.34	0.54	0.33	0.55	0.23	0.89	–	–
CATS	–	–	–	0.66	–	0.31	–	–	–
Ae	71.18	78.97	86.34	93.82	65.64	83.21	96.72	41.77	37.82
Wo	15.59	11.32	3.97	–	14.93	7.61	0.30	27.65	30.94
Fs	4.39	2.32	5.55	4.47	12.34	5.61	0.40	12.47	22.38
En	8.42	6.84	3.59	0.71	6.53	3.04	1.69	18.11	8.85

Projection from Wo into Ae-Hd-Di

	1	2	3	4	5	6	7	8	9
Ae	72.68	80.49	89.81	98.60	74.35	88.34	96.92	64.06	60.65
Hd	9.36	4.94	3.04	–	12.63	5.35	2.68	10.15	26.21
Di	17.96	14.57	7.15	1.40	13.03	6.30	0.40	25.79	13.14

FeO_T = total Fe calculated as FeO; n.d. = not detected; TiPx = $CaTiAl_2O_6$; CATS = $CaAl(Si,Al)O_6$; Ae = aegirine; Wo = wollastonite; Fs = ferrosilite; En = enstatite; Hd = hedenbergite; Di = diopside.
Compositions; 1–2, K-batisite syenite 237; 3, shcherbakovite-wadeite syenite 184/11; 4, eudialyte syenite; 5–6, tinguaite 127; 7, leucitophyre 230; 8–9, benstonite carbonatite.

Centre-IV. Pyroxene in centre-IV benstonite carbonatite occurs as prismatic euhedral-to-subhedral bright green diopsidic aegirine which exhibits a restricted range of composition (Table 4; Fig. 5). The pyroxene is TiO_2-poor (0.3–1.2 wt.%) and notably deficient in Al_2O_3 (not detectable by WDS microprobe) relative to less-evolved pyroxene in centres I and II. With respect to their aegirine contents they are more evolved than pyroxene from centres I and II but less evolved than pyroxene in centre III complex hypabyssal dykes and centre IV charoitites.
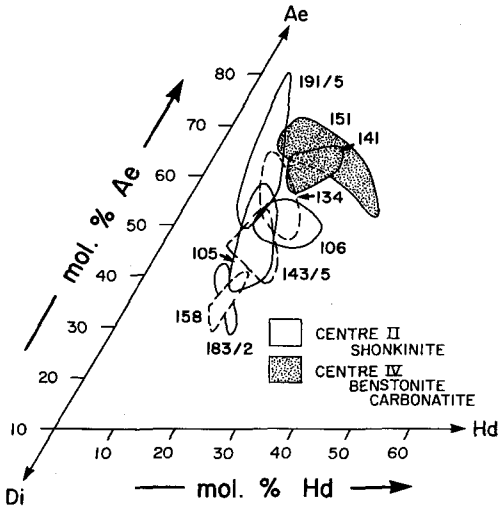
FIG. 5. Compositional variation of pyroxene in centre-II shonkinites and centre-IV benstonite carbonatites.

Pyroxene in rocks of the charoite complex form spectacular radial aggregates of prismatic aegirine (Ivanyuk and Evdokimov, 1991). These Al-poor (not detectable), relatively TiO_2-rich (0.8−1.8 wt.%) pyroxenes are considered by Ivanyuk and Evdokimov (1991) to contain significant amounts of $Na(Mg_{0.5}Ti_{0.5})Si_2O_6$ (4−10 mol.%). Assignment of Ti exclusively to this end-member rather than the Fe^{2+}-analogue is debatable, given the large number of potential end-member recalculation schemes which are possible for these compositions.

Compositional variation of mica

Representative compositions of mica from centre I and II rocks are given in Tables 5−7 and their compositional variation is illustrated in Figs 7−9. Mica is not present in centre-III effusives or titano- and zirconosilicate-bearing hypabyssal rocks. 'Lamproite-like' dyke rocks contain microphenocrystal and groundmass mica. Compositional data for some of these micas have been presented by Mitchell and Bergman (1991). Further data are provided in Table 8 and Figs 8 and 10.

127 - TINGUAITE - III
175 - EUDIALYTE SYENITE

236 - LAMPROPHYLLITE SYENITE - III
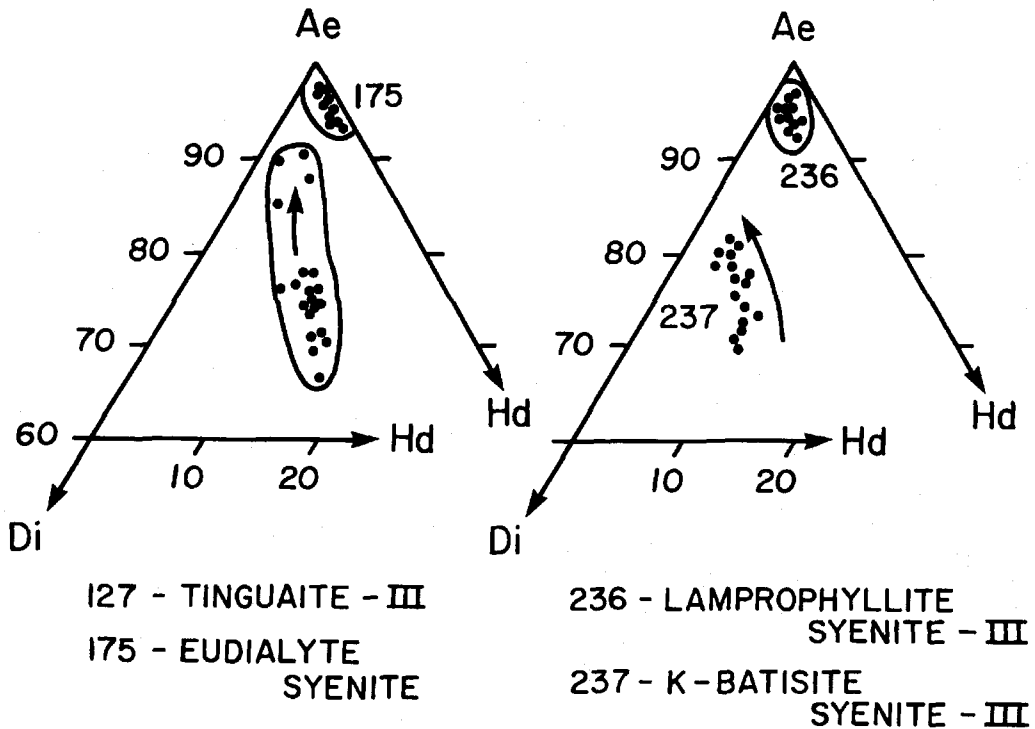237 - K-BATISITE SYENITE - III

FIG. 6. Compositional variation of pyroxene in centre-III tinguaite and late-stage mineralogically complex hypabyssal rocks.

TABLE 5. Representative compositions of phlogopite from centre-I phlogopite kalsilite syenites (yakutites)

wt.%	1	2	3	4	5	6	7
SiO_2	39.09	37.64	37.10	39.93	39.28	39.40	39.85
TiO_2	0.56	1.44	0.71	2.14	2.37	1.48	2.75
Al_2O_3	16.20	13.66	12.38	10.11	9.81	11.62	8.79
Cr_2O_3	n.d.	n.d.	0.10	0.18	n.d.	0.04	n.d.
FeO_T	4.54	13.74	15.71	11.14	14.06	12.14	14.23
MnO	0.04	0.24	0.21	0.09	0.15	0.17	0.19
MgO	25.03	17.91	18.01	20.94	19.51	20.35	19.10
Na_2O	0.11	n.d.	n.d.	n.d.	n.d.	n.d.	n.d.
K_2O	9.85	10.13	9.68	9.80	9.34	10.04	9.49
BaO	n.d.	0.68	0.82	0.71	0.94	0.16	0.38
Ni	n.d.	0.05	n.d.	0.07	0.10	0.08	0.02
Total	95.38	95.59	96.68	95.05	95.81	95.48	94.87

Recalculated compositions on the basis of stoichiometry

Fe_2O_3	4.07	—	1.77	—	0.94	1.07	—
FeO	0.88	13.74	14.12	11.14	13.21	11.18	14.23
Total	95.79	95.59	96.85	95.05	95.66	95.59	94.87

Structural formulae calculated on the basis of 22 oxygens

Si	5.489	5.639	5.534	5.921	5.871	5.810	5.999
Al	2.681	2.412	2.176	1.767	1.728	2.020	1.559
Ti	0.059	0.162	0.304	0.239	0.266	0.164	0.311
Cr	—	—	0.012	0.021	—	0.005	—
Fe^{3+}	0.429	—	0.198	—	0.106	0.119	—
Fe^{2+}	0.104	1.721	1.761	1.382	1.651	1.378	1.792
Mn	—	0.031	0.027	0.011	0.190	0.021	0.020
Mg	5.238	4.021	3.982	4.628	4.346	4.473	4.286
Na	0.030	—	—	—	—	—	—
K	1.764	1.936	1.842	1.854	1.781	1.889	1.823
Ba	—	0.040	0.048	0.041	0.055	0.009	0.022
Ni	—	—	0.006	0.008	0.012	0.009	0.002
mg#	0.908	0.700	0.670	0.770	0.712	0.749	0.705

FeO_T = Total Fe expressed as FeO; n.d. = not detected.
Composition 1 = monticellite olivine phlogopite pyroxenite Cha 1/225a; Panina *et al.*, 1989);
2–7 = yakutite (this work); 2–3 (Cha 229), 4–5 (Cha 172), 6–7 (Cha 187/2).

Centre-I. Mica in the majority of mica pyroxenites and kalsilite pyroxenites are of similar composition and are low Al_2O_3 (8.5–12.0 wt.%), FeO_T- rich phlogopite (mg# = 0.67– 0.80). Mica from individual samples shows very limited but distinct ranges in composition (Figs 7–9). One phlogopite kalsilite pyroxenite (yakutite; Cha 229) is enriched in Al, but not Mg, relative to other mica (Fig. 8). Only mica from monticellite-bearing rocks of uncertain origin (Panina *et al.*, 1989) are highly aluminous and approach the composition of phlogopite *sensu stricto*

(Fig. 7; mg# = 0.90). TiO_2 and BaO contents vary between samples and range from 0.7–3.4 and 0.1–1.5 wt.%, respectively. Cr_2O_3 and NiO are typically very low (<0.2 wt.%). Increasing Ti contents are positively correlated with increasing Ba contents. The overall compositional trend is one of decreasing Al_2O_3 and MgO with increasing FeO_T at essentially constant TiO_2, i.e. a phlogopite to tetraferriannite trend.

Mica in centre-I shonkinite is slightly depleted in Al_2O_3 (Fig. 7–8), but not markedly enriched in Fe

TABLE 6. Representative compositions phlogopite from centre-I phlogopite pyroxenite and shonkinite

wt.%	1	2	3	4	5	6	7	8
SiO_2	40.47	39.55	39.15	39.50	39.90	39.24	38.84	40.13
TiO_2	1.19	1.79	3.12	1.49	1.63	1.64	2.18	1.17
Al_2O_3	9.89	10.39	9.71	10.16	8.89	10.14	8.97	8.80
Cr_2O_3	0.03	0.07	0.20	0.16	0.08	0.04	0.03	0.02
FeO_T	10.44	12.18	12.92	14.71	15.67	13.27	16.29	16.76
MnO	0.21	0.15	0.21	0.34	0.34	0.32	0.47	0.37
MgO	22.73	20.29	19.14	18.52	18.04	19.07	17.55	17.90
Na_2O	0.06	n.d.	0.08	0.06	0.14	0.08	0.08	0.04
K_2O	9.91	10.19	10.12	10.16	10.12	9.72	9.25	9.95
BaO	0.16	0.56	0.37	0.27	0.13	0.83	1.04	0.36
NiO	0.10	0.05	n.d.	0.12	0.09	n.d.	0.09	0.03
Total	95.14	95.27	95.04	95.49	95.03	94.35	94.79	95.53

Recalculated compositions on the basis of stoichiometry

	1	2	3	4	5	6	7	8
Fe_2O_3	3.08	—	—	—	—	—	0.06	0.23
FeO	7.66	12.18	12.92	14.71	15.67	13.27	16.23	16.55
Total	95.50	95.27	95.27	95.49	95.03	94.35	94.80	95.55

Structural formulae calculated on the basis of 22 oxygens

	1	2	3	4	5	6	7	8
Si	5.907	5.893	5.876	5.939	6.051	5.941	5.954	6.078
Al	1.701	1.827	1.718	1.800	1.589	1.809	1.621	1.571
Ti	0.131	0.200	0.035	0.169	0.186	0.187	0.251	0.133
Cr	0.003	0.008	0.024	0.019	0.009	0.005	0.004	0.002
Fe^{3+}	0.338	—	—	—	—	—	0.007	0.027
Fe^{2+}	0.936	1.520	1.622	1.849	1.988	1.680	2.081	2.096
Mn	0.026	0.019	0.027	0.043	0.044	0.041	0.061	0.047
Mg	4.945	4.512	4.282	4.150	4.078	4.303	4.010	4.041
Na	0.017	—	0.023	0.018	0.041	0.024	0.024	0.012
K	1.845	1.939	1.938	1.949	1.958	1.877	1.809	1.922
Ba	0.009	0.033	0.022	0.016	0.008	0.049	0.062	0.021
Ni	0.012	0.006	—	0.015	0.011	—	0.011	0.004
mg#	0.795	0.748	0.725	0.692	0.672	0.719	0.658	0.656

FeO_T = Total Fe expressed as FeO; n.d. = not detected. Compositions: 1—5 phlogopite pyroxenites, 6—8 shonkinites; 1 (M1), 2 (Cha 187/3),3 (Cha 187/5), 4—5 (Cha 183), 6—7 (Cha 120/9), 8 (Cha 144/9).

(Fig. 8) relative to mica in phlogopite pyroxenite. Thus, their compositions overlap those of the latter (Table 6; Figs 7—9). TiO_2 (1.2—2.2 wt.%) and BaO (0.1—1.0 wt.%) contents are similar to those of mica in phlogopite pyroxenite.

Centre-II. Mica in centre-II shonkinite and potassic syenite is biotite (mg# = 0.66—0.37) which is poorer in Al_2O_3 than mica in centre-I rocks (Table 7; Figs 7—9). They are thus considered to be more evolved than the latter. Although individual samples exhibit a limited compositional range, the series as a whole shows considerable variation with respect to total Fe content (Fig. 8). Calculated Fe^{3+}

contents are typically low (Table 7). Increasing calculated minimum Fe^{3+} contents are correlated with decreasing Al and Mg contents suggesting that Al-poor micas contain significant amounts of the tetraferriannite component.

Centre-II biotite has TiO_2 contents (1—2 wt.%; Fig. 9) that are similar to those of mica in centre-I rocks. BaO contents range from typically not detectable to 0.2 wt.%, and rarely up to 0.4 wt.%. Na, Ca, Cr and Ni are typically not detectable.

Centre-III. Table 7 and Figs 8 and 10 show that 'lamproite-like' dyke rocks contain mica which is essentially indistinguishable from mica in the Murun
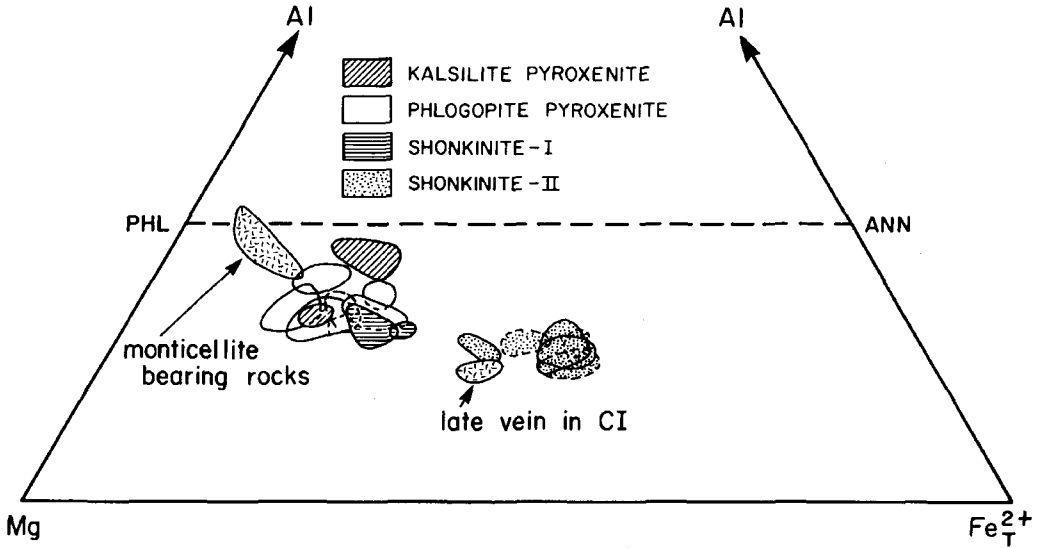
FIG. 7. Compositional variation of mica depicted in the ternary system Al—Mg—Fe$_T$. PHL = phlogopite; ANN = annite.

plutonic rocks. The principal difference is that some dykes contain mica which is slightly richer in TiO$_2$ (Fig.10). Individual dykes contain mica of distinct composition (Figs 8 and 10). Evolutionary trends are typically of decreasing Al and Mg with increasing Fe$_T$ and Ti. The degrees of Al depletion or Ti and Fe^{3+} enrichment (Figs 8 and 10) are not as great as found in mica from *bona fide* lamproites (Mitchell and Bergman, 1991).

Sample Cha-150 was originally described by Vladykin (1985) as a lamproite. This rock contains olivine macrocrysts which are mantled by colour-less amphibole and red-brown mica reaction rims together with mica phenocrysts which are identical to the latter. These minerals are set in a groundmass containing blue-green amphibole, red mica, Al-Ti-poor (<1 wt.%) diopside, apatite, Fe$_2$O$_3$- and BaO-poor (<1 wt.%) potassium
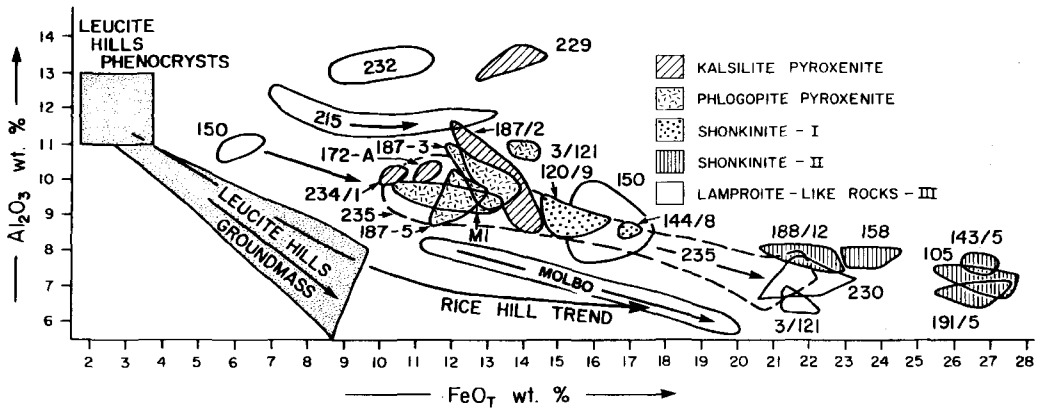
FIG. 8. Compositional variation, Al$_2$O$_3$ vs. FeO$_T$, for all Little Murun mica. Compositional trends for mica from Leucite Hills (Wyoming) and Rice Hill (Australia) lamproites from Mitchell and Bergman (1991).

TABLE 7. Representative compositions of biotite from centre-II shonkinites

wt.%	1	2	3	4	5	6
SiO_2	39.46	38.36	37.87	37.49	36.18	37.13
TiO_2	0.68	0.78	1.31	1.79	1.22	1.13
Al_2O_3	7.97	7.33	6.76	7.48	6.46	3.34
FeO_T	21.27	23.03	25.44	27.05	29.13	31.46
MnO	0.33	0.35	0.72	0.73	1.04	0.95
MgO	15.28	14.66	12.60	10.86	9.77	10.67
Na_2O	n.d.	n.d.	n.d.	0.09	0.07	0.02
K_2O	9.97	9.88	9.81	9.65	9.36	9.95
BaO	n.d.	0.16	n.d.	0.11	n.d.	0.10
Total	94.96	94.55	94.51	95.25	93.33	94.73

Recalculated compositions on the basis of stoichiometry

Fe_2O_3	1.39	3.25	2.39	0.61	3.59	5.80
FeO	20.02	20.11	23.29	26.50	25.89	26.24
Total	95.10	94.88	94.75	95.31	93.59	95.33

Structural formulae (22 oxygens)

Si	6.124	6.035	6.060	6.027	5.993	6.120
Al	1.458	1.359	1.275	1.417	1.261	0.649
Ti	0.079	0.092	0.158	0.216	0.152	0.140
Fe^{3+}	0.162	0.385	0.287	0.074	0.440	0.719
Fe^{2+}	2.599	2.645	3.117	3.563	3.587	3.618
Mn	0.044	0.047	0.098	0.099	0.146	0.133
Mg	3.535	3.438	3.005	2.602	2.412	2.612
Na	–	–	–	0.028	0.022	0.006
K	1.974	1.983	2.003	1.979	1.978	2.092
Ba	–	0.010	–	0.007	–	0.006
mg#	0.562	0.532	0.469	0.417	0.374	0.377

FeO_T = Total Fe expressed as FeO; n.d. = not detected.
Compositions; 1–2 (Cha 183/12), 3 and 6 (Cha 191/5), 4 (Cha 105), 5 (Cha 106).

feldspar, Fe-bearing calcite, rutile, baryte, rare chromite and magnetite.

Table 7 and Fig. 8 show that phenocrystal and reaction mica, in terms of Al and Fe content, represents some of the least evolved mica in the Murun complex. In contrast, groundmass mica is relatively depleted in Al and similar to evolved mica in centre-I shonkinites. The evolutionary trend is identical to that of mica in the plutonic rocks (Figs 8 and 10).

Also shown on Figs 8 and 10 are compositional data for mica from the Molbo dyke. This intrusion, whilst not a part of the Little Murun complex, is undoubtedly a part of the same spectrum of magmatic activity which gave rise to the Aldan ultrapotassic complexes and is considered to be a lamproite by many Russian petrologists (Makhotkin, 1991).

The dyke contains mica phenocrysts ranging in composition from phlogopite to biotite. The overall trend of compositional evolution is one of slightly decreasing Al coupled with increasing FeO_T and sightly increasing Ti. The trend lies parallel to that of the Little Murun mica but at lower Al contents. None of the mica in the Molbo dyke is compositionally similar to mica in bona fide lamproites. Pyroxene in the dyke is Al and Ti-poor and similar to diopside found in lamproites and pyroxene in the least evolved kalsilite and phlogopite pyroxenites. The data suggest that the Molbo dyke is related to Aldan ultrapotassic magmatism but is unlikely to be a bona-fide lamproite.

TABLE 8. Compositions of mica in centre-III lamproite-like rocks

wt.%	1	2	3	4	5	6	7	8	9	10
SiO_2	39.84	39.06	39.70	39.36	39.53	38.04	38.49	37.47	40.12	35.34
TiO_2	1.09	1.02	1.37	2.55	3.40	3.22	2.30	2.10	1.27	3.27
Al_2O_3	11.32	10.03	13.42	11.34	9.48	7.49	9.82	9.17	12.01	10.26
Cr_2O_3	0.38	0.25	0.62	n.d.	0.05	0.05	n.d.	n.d.	0.20	n.d.
FeO_T	6.34	16.03	8.93	14.75	9.98	21.53	11.64	19.56	7.34	26.69
MnO	0.06	0.39	0.04	0.05	0.07	0.44	0.11	0.43	0.04	0.24
MgO	24.74	18.32	22.09	17.61	22.09	15.02	21.59	16.39	23.75	9.59
Na_2O	0.09	0.02	0.03	0.10	0.13	0.12	0.14	0.07	0.05	0.07
K_2O	10.54	9.95	9.86	9.56	9.29	9.23	9.76	9.49	9.92	8.91
BaO	0.32	0.28	0.14	0.56	1.04	0.95	0.81	0.73	0.29	1.04
NiO	0.12	0.08	0.11	n.d.	0.09	0.04	0.09	n.d.	0.18	n.d.
Total	94.74	95.43	96.31	96.46	95.16	96.13	94.74	95.50	95.26	95.41

Recalculated compositions on the basis of stoichiometry

Fe_2O_3	2.12	2.13	1.29	—	—	0.64	2.54	3.04	2.03	—
FeO	4.43	14.11	7.77	14.75	9.98	20.98	9.35	16.82	5.51	26.69
Total	95.05	95.64	96.45	96.46	95.16	96.22	95.00	95.72	95.37	95.41

Structural formulae calculated on the basis of 22 oxygens

Si	5.772	5.883	5.697	5.865	5.845	5.908	5.740	5.764	5.784	5.703
Al	1.933	1.780	2.270	1.992	1.652	1.371	1.726	1.663	2.041	1.940
Ti	0.119	0.116	0.148	0.286	0.378	0.376	0.258	0.243	0.138	0.395
Cr	0.044	0.030	0.070	—	0.006	0.006	—	—	0.023	—
Fe^{2+}	0.231	0.242	0.140	—	—	0.075	0.285	0.352	0.220	—
Fe^{2+}	0.537	1.777	0.932	1.838	1.234	2.725	1.167	2.164	0.665	3.581
Mn	0.007	0.050	0.005	0.006	0.009	0.058	0.014	0.056	0.005	0.033
Mg	5.343	4.113	4.725	3.912	4.870	3.477	4.799	3.758	5.104	2.294
Na	0.025	0.006	0.008	0.029	0.037	0.036	0.040	0.021	0.014	0.022
K	1.948	1.912	1.805	1.817	1.753	1.829	1.857	1.862	1.824	1.824
Ba	0.018	0.017	0.008	0.033	0.060	0.058	0.047	0.044	0.016	0.065
Ni	0.014	0.010	0.013	—	0.010	0.005	0.011	—	0.021	—
mg#	0.874	0.671	0.586	0.680	0.800	0.554	0.768	0.599	0.852	0.388

FeO_T = total Fe expressed as FeO; n.d. = not detected. Compositions: 1–2, phenocryst and groundmass Cha 150; 3–4, zoned phenocryst Cha 232; 5–6, zoned phenocryst Cha 235; 7–8 phenocryst and groundmass Cha 241; 9–10, zoned phenocryst Cha 215.

Amphibole

Many of the centre-III 'lamproite-like' rocks contain microphenocrystal and groundmass blue-green amphiboles. These range in composition from magnesio-arfvedsonite to magnesio-riebeckite (Table 9). Compared with late-stage, lamproite-derived amphibole (TiO_2 = 3–5 wt.%; Ti>0.3 afu; Mitchell and Bergman, 1991) of similar major element composition, they are notably poor in TiO_2 (<0.4 wt.%; Ti<0.04 afu).

The Murun dyke (Cha-150) originally described as lamproite (Vladykin, 1985) contains colourless TiO_2 (0.3 wt.%)-poor potassium richterite in reaction coronas around olivine and blue-green potassium magnesio-arfvedsonite in the groundmass (Table 9). The paragenesis and composition of this richterite is atypical of lamproite amphiboles.

Colourless-to-blue-green, Ti-poor amphiboles also occur in some of the phlogopite pyroxenites. These are primary phases intergrown with diopside and phlogopite. The similarity in composition (Table 9)

TABLE 9. Representative compositions of amphibole in centre-III 'lamproite-like rocks' and centre-I pyroxenites

wt.%	1	2	3	4	5	6	7
SiO_2	55.18	56.27	52.96	57.74	55.98	56.69	55.19
TiO_2	0.20	0.23	0.32	0.31	0.12	0.26	0.38
Al_2O_3	0.32	0.32	0.37	0.01	0.85	0.79	0.39
FeO_T	11.89	20.24	10.86	1.14	6.15	6.26	12.09
MnO	0.40	0.08	0.39	0.08	0.16	0.16	0.93
MgO	15.99	12.00	16.55	23.43	20.15	20.23	15.61
CaO	3.09	1.49	3.57	6.53	6.00	10.87	2.58
Na_2O	5.75	6.27	5.54	4.19	5.18	2.02	5.77
K_2O	4.48	0.27	4.32	4.44	3.11	0.63	4.96
Total	97.36	97.17	94.88	97.87	97.70	97.91	97.90

Recalculated compositions on the basis of stoichiometry

Fe_2O_3	4.82	16.11	5.40	1.02	2.79	1.18	5.53
FeO	7.56	5.75	5.99	0.23	3.63	5.20	7.11
Total	97.78	98.73	95.44	97.97	97.98	98.03	98.45

Structural formulae calculated on the basis of 23 oxygens

Si	7.986	7.977	7.848	7.991	7.877	7.895	7.963
Al	0.014	0.023	0.065	0.002	0.123	0.105	0.037
Ti	—	—	0.036	0.007	—	—	—
Al	0.041	0.031	—	—	0.018	0.025	0.029
Ti	0.022	0.025	—	0.025	0.013	0.027	0.041
Fe^{3+}	0.531	1.718	0.624	0.106	0.298	0.123	0.601
Fe^{2+}	0.908	0.681	0.722	0.026	0.425	0.606	0.858
Mn	0.049	0.010	0.049	0.009	0.019	0.019	0.114
Mg	3.449	2.536	3.656	4.833	4.226	4.200	3.357
Ca	0.479	0.226	0.567	0.968	0.905	1.622	0.399
Na	1.521	1.723	1.433	1.032	1.095	0.378	1.601
Na	0.093	—	0.159	0.093	0.318	0.168	0.013
K	0.827	0.049	0.817	0.784	0.558	0.112	0.913
mg#	0.901	0.788	0.840	0.995	0.909	0.870	0.796

FeO_T = total Fe expressed as FeO. Compositions 1–4 'lamproite-like' rocks,
5–7 pyroxenites: 1, K-magnesio-arfvedsonite (Cha 141); 2, magnesio-riebeckite (Cha 232); 3, K-magnesio-arfvedsonite (Cha 150); 4, K-richterite (Cha 150); 5, K-richterite Cha 3/100); 6, actinolite (Cha 176/25); 7, K-magnesio-arfvedsonite (Cha 3/121).

of some, with the exception of Ti, to lamproite potassium richterite has led to suggestions that these rocks are plutonic lamproites (Shadenkov *et al.*, 1990). However, their host rocks do not contain any of the major typomorphic minerals of lamproites and are considered here to represent merely another modal variant of the kalsilite-phlogopite pyroxenite suite. Amphibole in other phlogopite pyroxenites is actinolite (Table 9). Such amphiboles are not found in lamproites (Mitchell and Bergman, 1991).

Discussion

Pyroxene and mica compositional trends confirm the sequence of formation of the Little Murun intrusive rocks proposed by Vladykin (1990) and Panina *et al.*
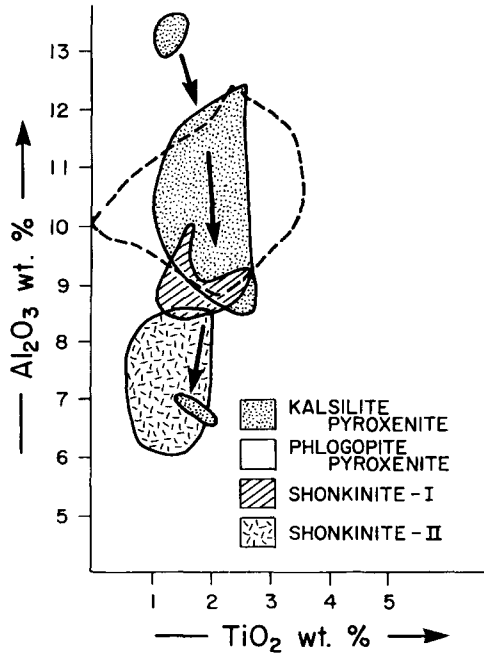
FIG. 9. Compositional fields, Al_2O_3 vs. TiO_2, for mica occurring in Little Murun plutonic rocks.

FIG. 10. Compositional fields, Al_2O_3 vs. TiO_2, for mica occurring in 'lamproite-like' hypabyssal rocks.

(1990). Mica in many of the plutonic rocks is relatively evolved compared with that in mica-rich hypabyssal rocks, suggesting that less-evolved portions of the intrusion may exist at depth. These undoubtedly give rise to the Martov gravity anomaly (Panina *et al.*, 1990) which underlies the principal outcrops of centre-I pyroxenites.

No significant differences are evident between the mica and pyroxene compositions of the kalsilite and phlogopite pyroxenites. This suggests that they are modal variants of rocks derived from a single magma type, with the kalsilite-bearing rocks representing slightly less-evolved fractions of the magma.

Lamproite-like hypabyssal rocks vary widely in character and may represent either early or late fractions of magmas tapped from evolving magma chambers at depths. They may be regarded as the lamprophyric facies (Mitchell, 1994) equivalents of the plutonic suite. The late-stage mineralogically-complex dykes represent the highly-evolved differentiates of several batches of compositionally distinct residual magmas. Unfortunately, discussion of the question of whether or not lamproites (*sensu* Mitchell and Bergman, 1991) are present in this complex is beyond the scope of this work.

The Little Murun pyroxene compositional trend is unusual in that it is essentially between diopside and

aegirine. Thus, pyroxene compositions in the ternary system diopside—aegirine- hedenbergite (Fig. 11) plot parallel to the diopside—aegirine join and contain less than 15 mol.% hedenbergite. This trend is unlike pyroxene compositional trends found in either undersaturated or saturated sodic alkaline complexes regardless of whether they are agpaitic or miascitic in character (Fig. 12). These data clearly demonstrate that the magma from which the Murun pyroxenes formed had a character that induced the formation of pyroxenes with very high Fe^{3+}/Fe^{2+} ratios but which simultaneously led to the crystallization of co-existing micas which were not similarly highly enriched in Fe^{3+}. Thus, micas highly-enriched in tetraferriannite do not co-exist with aegirine and tetraferriphlogopite does not form. These observations suggest that the magma bulk composition played a greater role in determining the compositions of the minerals crystallizing than
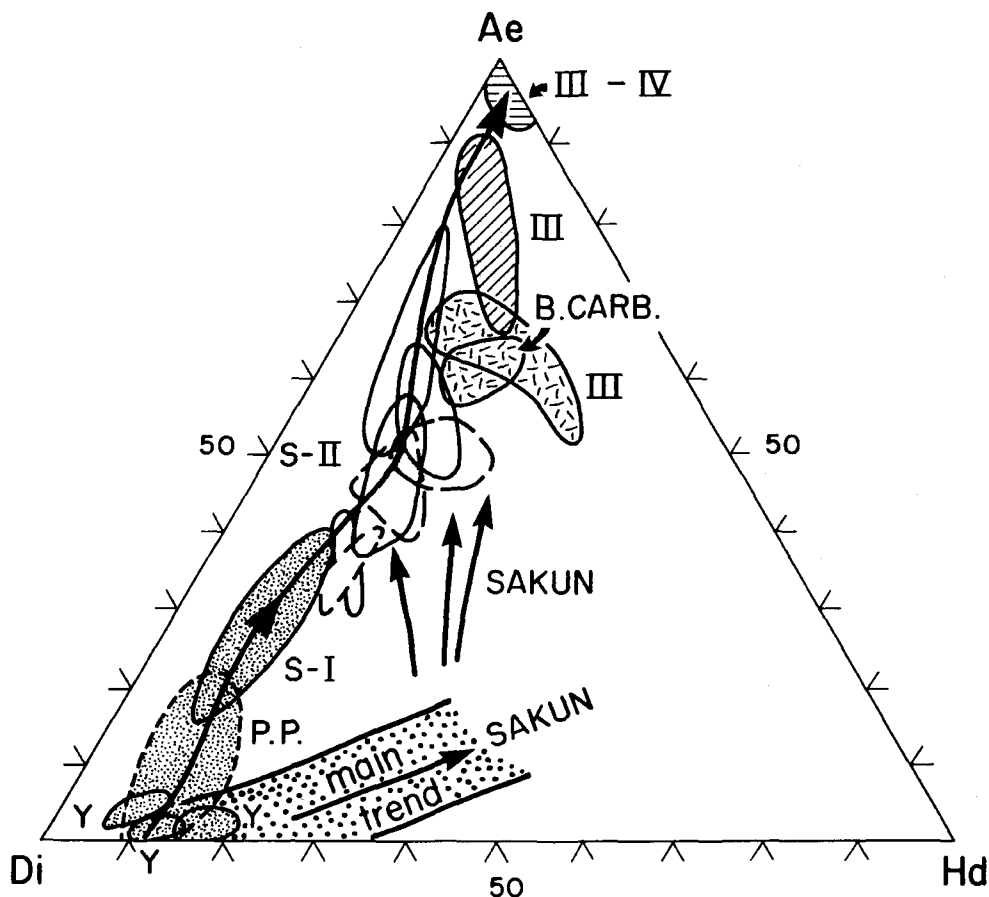
FIG. 11. Overall compositional trend (mol.%) of pyroxene occurring in Little Murun plutonic rocks depicted in the ternary system aegirine (Ae)- diopside (Di) - hedenbergite (Hd). Y = yakutite (kalsilite pyroxenite); P.P. = phlogopite pyroxenite; S = shonkinite. B.CARB = benstonite carbonatite. Roman numerals indicate plutonic centres. Compositional trends for Sakun potassic complex (Aldan Shield) pyroxenes from Proshenkin and Sharygin (1990).

oxygen fugacities. Note, it is not possible to estimate oxygen fugacities of the magma, as common iron-titanium oxides are absent and thermodynamic data for minerals which might serve as potential oxygen buffers are not available.

The Sakun complex, also located in the Aldan Shield, is the only other ultrapotassic complex for which significant amounts of pyroxene compositional data are available (Proshenkin and Sharygin, 1990). Figure 11 shows that the Sakun pyroxene compositional trend is similar to those of sodic alkaline complexes and not to that of the Little Murun complex. This observation further emphasizes the unique character of the magmas from which the Murun complex was formed.

Conclusions

The principal conclusions of this study are that: (1) Pyroxene and mica compositional trends may be used to place individual units of the Little Murun complex in their correct petrogenetic sequence of formation. (2) The pyroxene compositional trend exhibited by plutonic rocks of the Little Murun ultrapotassic complex is unique.
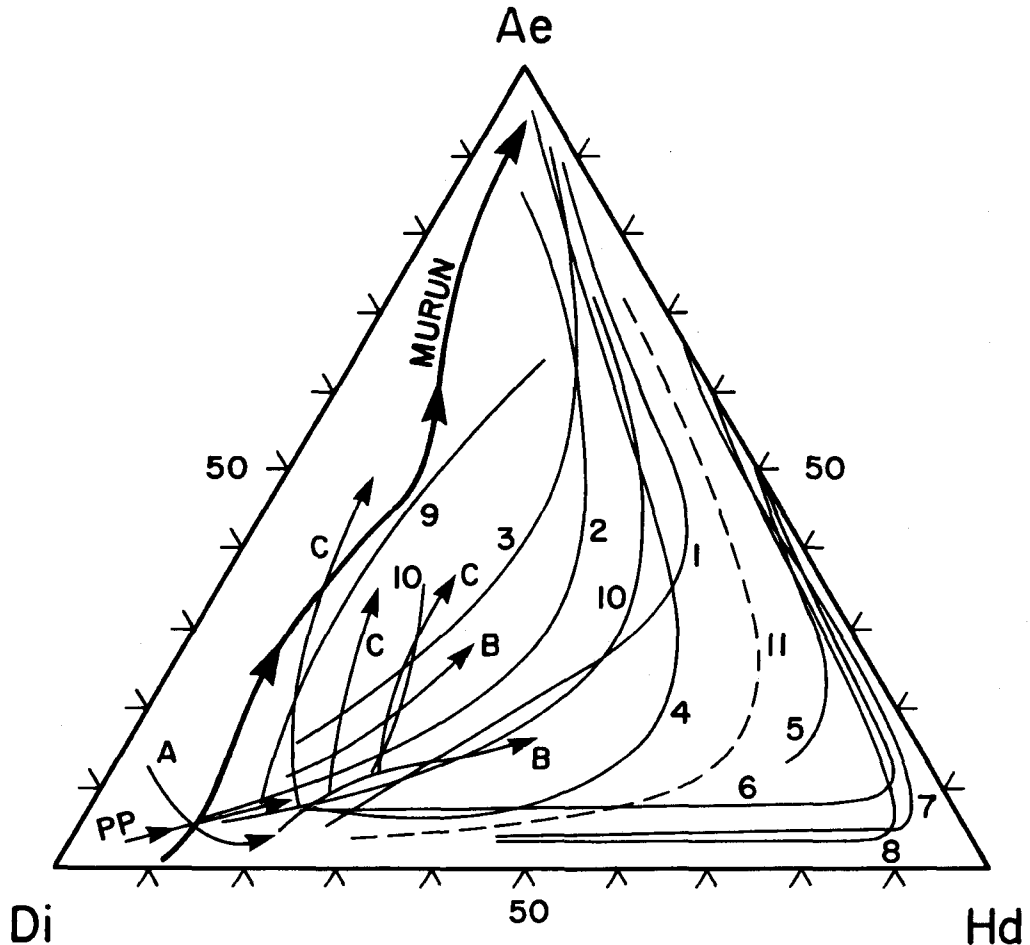
Acknowledgements

FIG. 12. Overall trend of pyroxene compositions (mol.%) in the Little Murun ultrapotassic complex compared with trends found in other alkaline rocks: 1 Morotu; 2 Uganda; 3 Itapirapua; 4 South Qoroq; 5 pantellerite; 6 Nandewar; 7 Ilimaussaq; 8 Coldwell centre-I; 9 Turja; 10 Iron Hill; 11 Coldwell-II; A,B,C, Fen. See Mitchell and Platt (1982) for data sources.

References

Alekseyev, Y.A. (1983) Geology of new types of carbonatites and associated rocks. *Dokl. Akad. Nauk SSSR*, **272**, 134–7.

Bilibina, T.V., Daskova, A.D., Donakov, V.I. Titov, V.K., and Shchukin, S.N.(1967) *Petrologiya shchelochnogo vulkanogenno-intruzivnogo kompleksa Aldanskogo shchita (Petrology of the Alkaline Volcanic Intrusive Complexes of the Aldan Shield)*. Nedra Press, Leningrad.

Biryukov, V.M. and Berdnikov, N.V. (1993) The paragenetic relation between charoite mineralization and alkali metasomatism. *Internat. Geol. Rev.*, **35**, 585–602.

Droop, G.T.R. (1987) A general equation for estimating Fe^{3+} concentrations in ferromagnesian silicates and oxides from microprobe analyses using stoichiometric criteria. *Mineral. Mag.*, **51**, 431–5.

Ivanyuk, G.Y. and Evdokimov, M.D. (1991) Pirokseny

charoitogo mestorozhdeniya Sirenevyy Kamen i nekotorye zakonomernosti ikh obrazovaniya (Pyroxenes from the charoitic ore deposit Sirenevii Kamen and some observations on their genesis) *Zap. Vses. Mineral. Obshch.*, **120**, 62—74 (Russian).

Kogarko, L.N., Kononova, V.A., Orlova, M.P. and Woolley, A.R. (1995) *Alkaline Rocks and Carbonatites of the World Part 2: Former USSR.* Chapman & Hall, London.

Konyev, A.A., Vorobyev, Y.I. and Bulakh, A.G. (1993). Charoit - der Schmuckstein aus Sibirien und sine seltenen Begleitminerale. *Lapis*, 13—20.

Kostyuk, V.P., Panina, L.I., Zhidkov, A.Y., Orlova, M.P. and Bazarova, T.Y. (1990) *Kalievii shchelochnoi magmatizm Baikalo-Stanovoi riftogennoi sistemy* (Potassic Alkaline Magmatism of the Baikal-Stanovoy Rifting System) Nauka Press, Novosibirsk (Russian).

Makhotkin, I.L. (1991) Lamproity Aldanskoi provintzii (Lamproites of the Aldan province) In: *Lamproity (Lamproites)* (O.A. Bogatikov, I.D. Ryabchikov and V.A. Kononova, Eds.) Nauka Press, Moscow, pp. 46—113.

Mitchell, R.H. (1980) Pyroxenes of the Fen alkaline complex, Norway. *Amer. Mineral.*, **65**, 45—54.

Mitchell, R.H. (1994) The lamprophyre facies. *Mineral. Petrol.*, **51**, 137—46.

Mitchell, R.H. and Bergman, S.C. (1991) *Petrology of Lamproites.* Plenum Press, New York.

Mitchell, R.H. and Platt, R.G. (1982) Mineralogy and petrology of nepheline syenites from the Coldwell alkaline complex, Ontario, Canada. *J. Petrol.*, **23**, 186—214.

Orlova, M.P. (1988) Recent finding on the geology of the Malo Murun alkaline pluton. *Internat. Geol. Review*, **30**, 945—53.

Orlova, M.P., Borisov, A.B. and Shadenkov, Y.M. (1992) Alkaline magmatism of the Murun areal (*sic*) (Aldan Shield). *Sov. Geol Geophys.*, **33**, 45—55.

Panina, L.I., Motorina, I.V., Sharygin, V.V. and Vladykin, N.V (1989) Biotitic pyroxenites and melilite-monticellite-olivine rocks of the Malo Murun alkaline massif of Yakutia. *Geol. Geophys.*, **30**, 40—8.

Panina, L.I., Sharygin, V.V. and Motorina, L.V. (1990) Mica pyroxenites as products of early stages of evolution of potassium alkali magma (on the example of the Malomurun alkali massif, Aldan shield). *Geol. Geophys.*, **31**, 68—74.

Prokofiev, V.Y. and Vorobyev, Y.I. (1992) P-T formation conditions for Sr-Ba carbonatites, charoite rocks and torgolites in the Murun alkali intrusion, east Siberia. *Internat. Geol. Rev.*, 83—92.

Proshenkin, I.E. and Sharygin, V.V. (1990) Features of the composition of pyroxenes of the Sakun massif. *Geol. Geophys.*, **31**, 51—6.

Shadenkov, Y.M., Orlova, M.P. and Brisov, A.B. (1990) Pyroxenite and shonkinites of the Malo Murun pluton: intrusive analogs of lamproite. *Internat. Geol. Rev.*, **32**, 61—9.

Smyslov, S.A. (1986) Kalsilite-bearing rocks of the Malomurun massif. *Geol. Geophys.*, **27**, 30—4.

Tyler, R.C. and King, B.C. (1967) The pyroxenes of the alkaline igneous complexes of eastern Uganda. *Mineral. Mag.*, **36**, 5—22.

Vladykin, N.V. (1985) First find of lamproites in the USSR. *Dokl. Akad. Nauk SSSR*, **280**, 718—22.

Vladykin, N.V. (1990) On the genesis of charoite rocks. *Proc. 15th. General Meeting Internat. Mineral. Assoc. Beijing.* Abstracts, **2**, 689—90.

Zhidkov, A. Y. and Smyslov, S.A. (1985) Some distinctive features of synnyrites and the typochemistry of the minerals forming them. *Geol. Geophys.*, **26**, 31—9.